Characterizing permafrost valley fills along the Alaska Highway, southwest Yukon

Joel Pumple[1], Duane Froese[1], & Fabrice Calmels[2]
[1]*University of Alberta, Edmonton, AB, Canada*
[2]*Yukon Research Centre, Yukon College, Whitehorse, YT, Canada*

GEOQuébec 2015
Challenges from North to South
Des défis du Nord au Sud

ABSTRACT
In the Beaver Creek area of southwest Yukon, the Alaska Highway traverses both glaciated and non-glaciated terrain from the Last Glacial Maximum. In this area permafrost characteristics are strongly influenced by regional glacial history including the distribution of relict Pleistocene permafrost. Here we characterize the distribution and history of permafrost in a valley fill along the Alaska Highway between Beaver Creek and the Alaska border using a multidisciplinary approach. Our surveys include Electrical Resistivity Tomography (ERT), permafrost drilling, cryostratigraphy, and geochemical analyses to define the boundaries and characteristics of the valley fill. Using ERT data we mapped the widespread distribution of ice-rich organic silts of Holocene age that unconformably overlie relict syngenetic permafrost from the Late Pleistocene within the valley fill. Radiocarbon dating and stable isotope analyses of $\delta^{18}O$ and δD, combined with detailed cryostratigraphy, confirm the presence of relict syngenetic ground ice from the Late Pleistocene (>57,000 14C years BP), indicating the considerable antiquity of ice-rich permafrost at this southerly locality.

RESUME
À proximité de Beaver Creek, au sud-ouest du Yukon, la route de l'Alaska traverse à la fois des terrains qui furent recouverts de glace et d'autres non lors du dernier maximum glaciaire. Dans cette région, les caractéristiques du pergélisol sont fortement influencées par l'histoire glaciaire locale incluant la distribution du pergélisol relique du Pléistocène. Ici, la distribution et l'histoire du pergélisol dans les remplissages d'une vallée le long de la route de l'Alaska entre Beaver Creek et la frontière alaskienne sont caractérisées en utilisant une approche multidisciplinaire. Dans le but de définir les limites et les caractéristiques de ces dépôts de fond de vallée, l'étude comprend des levés de tomographie électrique (ERT), des forages, ainsi que des analyses cryostratigraphiques et géochimiques. Les données ERT permettent de cartographier la distribution du pergélisol syngénétique relique du Pléistocène supérieur dans de la vallée, où des dépôts reliques ont été dégradés puis ont été recouverts de sédiments organiques durant l'Holocène. Les datations au radiocarbone et les analyses des isotopes stables $\delta^{18}O$ et δD combinées aux cryostratigraphies détaillées confirment que la plupart de la glace de sol est relique du Pléistocène supérieur.

1 INTRODUCTION

Low relief valley fills with extensive organic-rich soils and wetlands are common features in the lowland areas of unglaciated Yukon and Alaska (Jensen et *al*., 2009; Kanevskiy et *al.*, 2014). These plains and lowlands may be composed of eolian, alluvial, lacustrine, and organic sediments (Froese 2005) and may record complex local histories of sedimentation. In this paper we investigate a single low relief valley fill in southern Yukon using a combination of borehole data and Electrical Resistivity Tomography (ERT) surveys.

The Alaska Highway traverses southern Yukon in the discontinuous permafrost zone (Smith and Riseborough, 2002; Throop et *al.* 2012). Between Beaver Creek and the Alaska border, the highway is constructed on both syngenetic and epigenetic permafrost. In areas of syngenetic permafrost ice volume tends to be greater than in areas of epigenetic permafrost with a distribution related to the past climate and sedimentation history at the time of formation. In the non-glaciated areas, where eolian sedimentation took place during the Late Pleistocene, ice volumes may approach 50% of the subsurface where syngenetic ice wedges accompanied aggradation (Kanevskiy et al. 2011; Schirrmeister et al., 2013). The geochemical, geochronological, and cryostratigraphical aspects of permafrost are important in understanding its origins and paleoclimatic significance (Burn et al. 1986).
Understanding ground ice distribution along the Alaska Highway is crucial when considering continued highway maintenance and construction under a warming climate (Opel, et *al*. 2011; Throop, et a*l.* 2012).

Permafrost samples collected from borehole exploration provide an opportunity to investigate each of the fore mentioned aspects. Stable isotope ratios of $\delta^{18}O$ and δD from ice-rich permafrost samples and radiocarbon dating of organic-rich samples provide details about the paleoclimate in the region (Lacelle et *al.* 2009). The use of detailed cryostratigraphic interpretations offers a better understanding of permafrost genetic history (Murton and French 1994; Bray et *al.* 2006; French and Shur 2010). In this study, we use borehole data combined with ERT surveys to interpret the distribution and extent of permafrost. Using this combined approach, we utilize the borehole and ERT data to: (1) map the distribution of ice-rich permafrost in a lowland valley-fill along the Alaska

Highway; and (2) determine the age of the ice rich permafrost within the valley fill.

2 STUDY AREA

The study area is located in Southwestern Yukon, ten kilometres north of Beaver Creek along the Alaska Highway in the discontinuous permafrost zone (Fig. 1). This region is an area of meta-stable warm permafrost (Throop et *al.* 2012), making it a suitable area to study permafrost as it approaches thaw temperatures. The dominant vegetation cover in the study area is a combination of moss-sphagnum and sedge-tussock communities, often coupled with low-density black spruce. The Last Glacial Maximum (LGM) limit, as mapped by Duk-Rodkin (1999), cross cuts the Alaska Highway ~5 km south of Beaver Creek. It is assumed that terrain south of the limit is glacially influenced and material north is influenced more by periglacial processes associated with the proglacial and extraglacial environment.

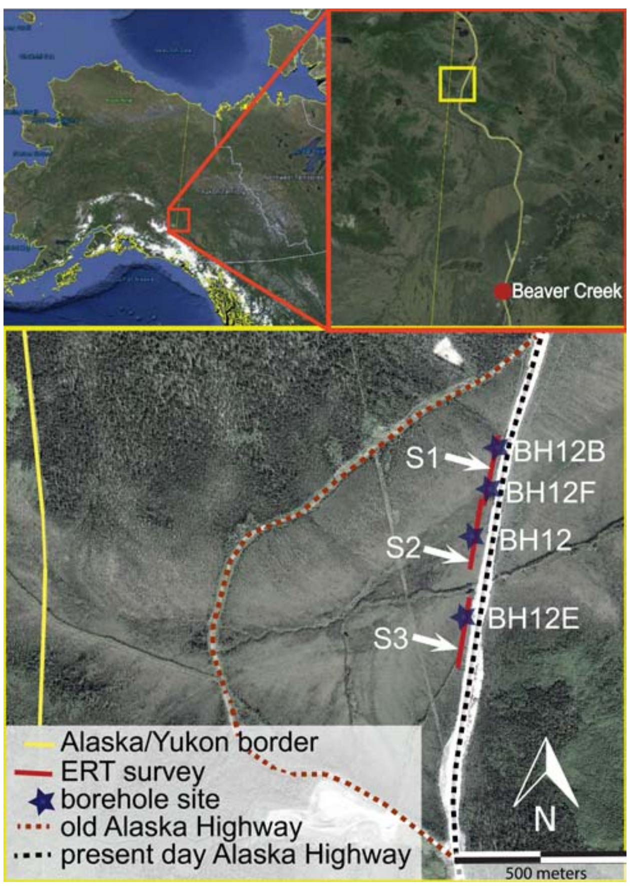

Figure 1. Map of the study area using images captured from google earth (Data SIO, NOAA, U.S. Navy, NGA, GEBCO, Image © 2015 DigitalGlobe, © 2015 Google, Image Landsat, Image IBCAO). The lower panel is indicated in the upper right panel by the yellow box.

3 METHODOLOGY

This project uses a multidisciplinary approach including geophysical surveys, geochemical analyses and geomorphological interpretations. In total four boreholes were drilled and three ERT surveys completed within the study area (Fig. 1). The three electrical resistivity tomography (ERT) surveys (S1, S2 and S3; Fig. 1) were collected with an Iris Syscal Junior switch 48, using a Wenner array. One profile was collected in the valley bottom and one on both north and south valley walls. Each survey used 48 electrodes with a 5 metre spacing for a total survey length of 235 metres and, using the Wenner array, reached a depth of 42 metres. The surveys were inverted using RES2DINV (Loke and Barker 1996). Out of the four boreholes drilled, two were collected in the valley bottom and one on either valley wall. Each borehole intersected an ERT survey to allow for ground truthing of the ERT results. The boreholes were drilled using a portable earth drill (Calmels, et *al.* 2005) and collected cores were then stored in a portable cooler on site and at the end of the day transferred to a deep freeze for storage until they could be returned to the lab. At the University of Alberta the cores were sampled for grain size analyses, ice volume content, water isotopic analyses, organic matter for radiocarbon dating, and volcanic ash, where present, for electron microprobe analyses using established methods (Jensen et *al.* 2008). Ice volume measurements were carried out using a half section of the core in order to keep a clean sample for isotope analyses. The half section of core was submerged in 1.5 litres of cold water housed in a 4 inch diameter PVC pipe and the displaced water was drained and measured with a 250 ml graduated cylinder. The ice volumes reported include pore ice. Water isotope analyses were completed on a Picarro L2130-*i* water isotope analyzer in the Department of Earth and Atmospheric Sciences at the Univeristy of Alberta. The $\delta D/\delta^{18}O$ values were calibrated to VSMOW based on two standards (USGS 45 and USGS 46) run at the same time as the unknowns. Measurement precision in this study is 1.0‰ for δD and 0.2‰ for $\delta^{18}O$ based on routine measurement of an internal lab standard. Radiocarbon samples were prepared using an Acid-Base-Acid pre-treatment at the University of Alberta and analyzed at the Keck Accelerator Mass Spectrometry Lab at the University of California, Irvine. Cryostratigraphic interpretations were completed on each core using a slightly modified version of the classification scheme outlined in Murton and French, 1994 (Fig. 2).

4 RESULTS

4.1 Cryostratigraphy

Seven cryofacies were defined based on cryostructures, ice content, grain size, sediment type, and orientation of the sedimentary layers (Fig. 2). Throughout the valley fill cryofacies two (Organic-rich, ice-poor sandy silt) and zero (ice-rich peat) repeat in each borehole with the exception of the southern borehole BH12E where cryofacies zero is absent. BH12E is the only borehole that contains cryofacies four (ice-poor organic-rich sandy silt), five (sediment-rich ice) and six (sediment-poor ice) Two cryofacies assemblages have been identified based on repeating patterns or significant lithological or geochemical

Cryofacies

#	Description
0	Ice-rich structureless peat with visible wood fragments suspended in peat and crustal cryostructure.
1	Ice-rich cryoturbated to flat lying peat or organic-rich sandy silts; may contain ash, wood fragments, and gravel. Sandy silts have parallel layered (0.2-2.5 cm thick) or non-parallel wavy lenticular ice (0.1-0.8 cm thick). Peat displays non-parallel wavy lenticular (0.3-1.2 cm thick). Ash (if present) and sand or gravel rich layers are structureless. Crustal cryostructure commonly surrounds wood fragments.
2	Flat lying to cryoturbated sandy silt with variable organic content, gravel, peat, ash (if present) and wood fragments with moderate to low ice content. Vertical and horizontal ice layers (0.1-1.1cm thick) visible throughout. Silt contains non-parallel wavy lenticular (0.3-6.0 mm thick). Sections of peat are structureless to parallel wavy lenticular (0.1-1.0 cm thick) and wood fragments have a crustal cryostructure. Ash and coarse sandy silt are structureless.
3	Ice-poor sandy silt with gravel; structureless cryostructure.
4	Cryoturbated ice-poor structureless grey sandy silt, organic silt, and wood fragments throughout.
5	Sediment-rich ice with suspended brown silt; pool ice or karst ice.
6	Foliated sediment-poor ice with subvertical gas bubble foliations; ice wedge ice.

Figure 2. Images and descriptions of each cryofacies found in the study area. The classification scheme outlined by Murton and French (1994) guided these results.

changes. Cryofacies assemblage one, upper unit, is defined by a repetition or presence of cryofacies zero, one and two. Cryofacies assemblage two, lower unit, consists of cryofacies three through six.

4.2 Grain Size And Ice Volume

The sediments primarily consist of silt and clay with smaller components of sand and gravel. The ice volume content in the two valley bottom boreholes (BH12 and BH12F) is greater on average than the valley wall boreholes (BH12E and BH12B). The valley wall boreholes BH12E and BH12B have similar ice volume content throughout (Fig. 3).

4.3 Stable Isotopes

The isotopic ratios of pore ice sampled from the boreholes typically range from -19.5 to -22.4 ‰ $\delta^{18}O$ and -155 to -177 ‰ for δD. These values are typical for all cores except for the bottom two cores from BH12B and the bottom half of BH12E, where more depleted isotopic ratios were sampled with values between -23‰ and –27‰ for $\delta^{18}O$, and -180‰ to -220‰ for δD (Fig. 3).

4.4 Chronology

Each borehole contained a layer of the eastern lobe of the White River Ash (A.D. 833–850) in the top two metres but no other ash layers at greater depths (Jensen, et *al*., 2014). Radiocarbon dates are plotted in Figure 3 and Table 1. Radiocarbon dates from below ~3.5 metres depth at BH12E are beyond the limit of radiocarbon dating, giving non-finite results. All radiocarbon samples were >.3mg except one as seen in Table 1. Small mass standard FIRI-F (AKA FIRI-D ca 4510 ^{14}C yr BP; Boaretto et *al*. 2002) is within error of its expected value (Table 1). The samples were also run with a non-finite standard

AVR-07-PAL-37 (Reyes et al. 2010). Previous work has shown that robust woody samples from similar sediments may yield inaccurate age estimations due to reworking of the organic material (Kennedy et al. 2010). Radiocarbon dates from BH12B date to the early Holocene 8450-9245 Cal years BP

Table 1. Radiocarbon dates including calibrated one sigma range, non-calibrated result, error and lab (UCIAMS) number. Dates were calibrated using Calib ver. 7.1 with the intCal13 calibration curve (Reimer et *al.* 2013).

UCIAMS #	Sample	Material	^{14}C age (BP)	±	Cal ^{14}C age (BP) range
156126	BH12F-386	wood	6960	15	7760-7830
142056	BH12-433	wood	4555	20	5140-5310
156127	BH12B-191	wood	3810	15	4155-4230
156134	BH12B-264	wood	4720	20	5330-5575
156133	BH12B-385	wood	7335	15	8060-8180
156130	BH12B-485 .013mgC	grass	7960	330	8450-9245
156128	BH12E-191	wood	6385	20	7270-7406
156138	BH12E-358	wood	>50800		
156139	BH12E-466	wood	>55500		
156131	FIRI-F .015mgC	wood	4670	150	
156132	FIRI-F	wood	4540	15	
156136	AVR-07-PAL-37	wood	51500	370	
156137	AVR-07-PAL-37 .013mgC	wood	24230	300	

(485 cm depth) and 8140 8060-8180 Cal years BP (385 cm depth; Fig. 3 and Table 1).

4.5 Geophysical Surveys

The ERT surveys provide a two-dimensional view of the resistivity properties of the subsurface (Lewkowicz et al. 2011). The base of the active layer is not visible in the surveys due to the large electrode spacing, however from ~1.25 metres depth onwards ground resistivity values are resolved in the model. The top of each survey shows a heterogeneous layer in terms of resistance, with values varying between 400 and 7000 ohm-m. This variable top layer ranges in thickness from ca. 3 -20 metres, and typically overlies a higher resistivity layer. The high resistivity (~12,000 ohm-m) layer varies between 10 and 25 metres in thickness and is present at 6.25, 5.5, and 5.5 metres depth at the north, bottom, and south valley sites, respectively (Fig. 4). The lower deposits of both valley wall surveys are dominated by a thick laterally continuous layer of lower resistance (~1200 ohm-m). This layer dips towards the valley bottom in both surveys and is between 14 and 35 metres thick (Fig. 4).

5 DISCUSSION

The cryostratigraphic investigation highlighted that the majority of the boreholes contain repeating layers of organic-rich sandy silts (cryofacies 2) and peat (cryofacies 0) (Fig. 3). This repeating pattern is common in permafrost sediments where the peat layers mark periods of a stable surface with moist conditions allowing for establishment of vegetation and the sediment layers form during sedimentation events by fluvial, eolian or colluvial deposition (Fraser and Burn 1997). Rampton (1978) recorded similar results (sections, 4-A07 and 4-A08) in the study area while mapping surficial geology of the region. Organic material taken from the basal section within the upper unit dates to the early Holocene in both BH12E (7270-7406cal yrs BP; UCIAMS-156128) and BH12B (8450-9245cal yrs BP; UCIAMS-156130). Isotopes from this unit are typical of Holocene pore ice (> -23 ‰ δ^{18}O, Fig. 3; Kotler and Burn 2000). Several ice wedges were encountered during test boreholes and road maintenance within this upper unit throughout the valley with the exception of the northern valley slope. ERT results also show the localized near surface high resistivity ice wedge bodies in the valley bottom section (Figure 4).

Beginning at 2.9 and 5 metres depth in BH12E and BH12B, respectively, cryofacies three marks the transition to Late Pleistocene permafrost sediments in the lower unit (Fig. 3). Cryofacies three consists of ice-poor sandy silt and gravel exhibiting a structureless cryostructure throughout (Fig. 2). Within BH12B cryofacies three contains a large vertical reticulate ice vein (40 cm long and 1cm thick) must likely as a result of thawing ice rich permafrost and subsequent refreezing in a semi-closed freezing system (Mackay 1973). Coincident with cryofacies three is a marked trend toward more depleted isotope values that are typical of Late Pleistocene conditions (< -24 ‰ δ 18O, Fig. 3; Kotler and Burn 2000). These depleted isotope values, associated with cryofacies three, mark the stratigraphic transition from polygenetic Holocene permafrost to syngenetic Late Pleistocene permafrost. Cryofacies four is made up of cryoturbated ice-poor structureless organic grey sandy silt with wood fragments throughout. Radiocarbon dates taken from this cryofacies were non-finite suggesting deposition occurred prior to or concurrent with Reid-McConnell interglacial period (Hopkins 1982). Non-finite radiocarbon dates indicate a minimum age for the unit of >57000 14C age (BP). Cryofacies five and six

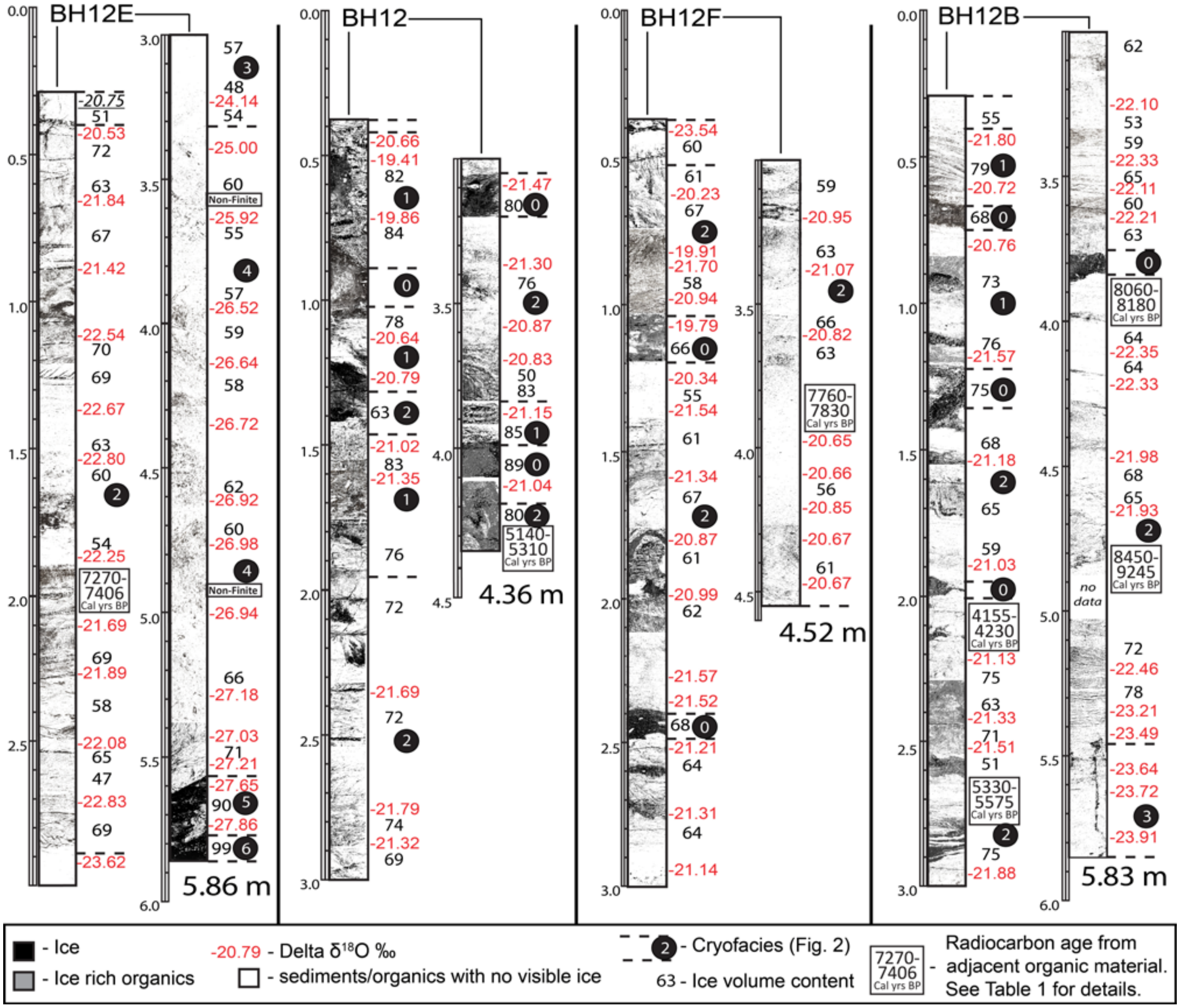

Figure 3. Four picture logs adjusted using Photoshop to highlight visible ice in black. The logs are presented in order from south (left) to north (right) across the valley.

comprise of sediment-rich pool ice and sediment-poor ice wedge ice, respectively. The isotopic values, cryostructures, and radiocarbon dates from cryofacies four, five and six together indicate an origin typical of Pleistocene silts found across unglaciated Yukon and Alaska (Froese et al. 2009; Schirrmeister et al. 2013). Sharply overlying these deposits and dating to the early Holocene are organic rich silts that mark the re-aggradation of permafrost following thaw degradation. Cryostratigraphic analyses reveal that cryofacies three most likely represents a paleo-thaw unconformity based on the structureless cryostructure, change in water isotope values and non-conformable radiocarbon dates above and below (Kotler and Burn 2000; French and Shur 2010). This unconformity records thermal degradation and removal of the Late Pleistocene material which would have been deposited prior to and during the McConnell Glaciation (Jackson et *al*. 1991; Kotler and Burn 2000; Jorgenson et *al*. 2010; Reyes et *al*. 2010). This process would have continued until the active layer stabilized in Holocene sediments. The natural thickening of sediments in the valley bottom compounded with the shallow boreholes collected from the valley bottom, suggest that the Pleistocene permafrost is only present near the valley walls and to a greater extent on the southern (north-facing) slope. However, the ERT results suggest that the highly resistive Pleistocene permafrost persists throughout the valley bottom at depth.

Three electrical resistivity tomography surveys spanning the valley section parallel to the highway provide an improved image of the distribution of permafrost (Fig. 1 and Fig. 4). A high resistivity layer present at depth throughout each survey is interpreted as relict Late Pleistocene syngenetic permafrost and this is supported by the valley wall boreholes BH12E and BH12B (Fig. 3 and

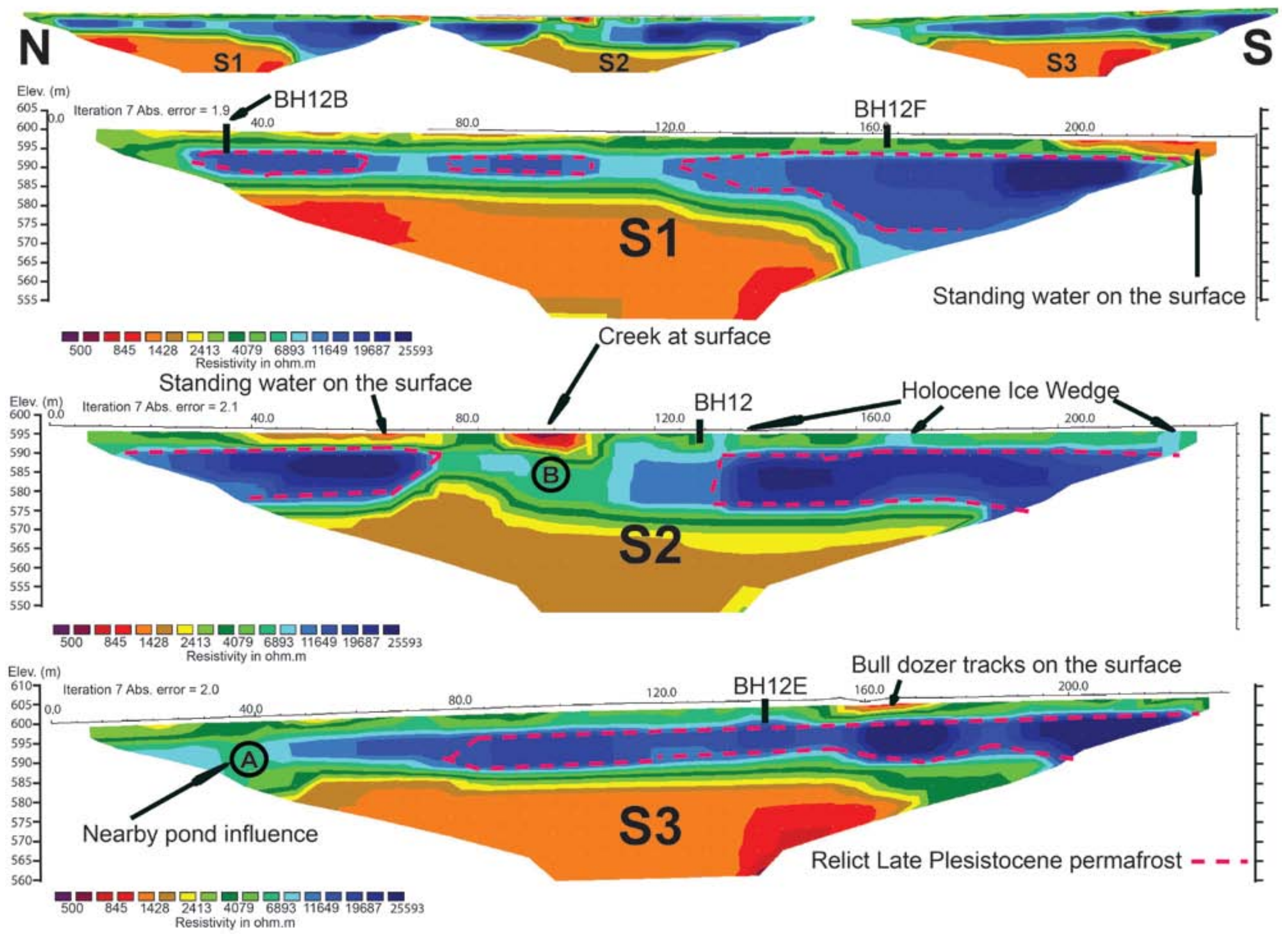

Figure 4: Electrical resistivity tomography results for the three surveys done across the valley from north to south. All surveys used 48 electrodes at 5 metre spacing and have an Abs. error <2.2.

Fig. 4). In the southern survey, at 5.5 metres depth, this layer was sampled in BH12E and includes an ice body at ~5.6 metres depth. Direct sampling of this layer provides a ground truthing for the ERT surveys. At position "A" in figure 4, the high resistivity layer is absent ~45 metres along the profile. As seen in figure 1 the first electrode of the survey (S3) was placed within a few metres of a small pond adjacent to the highway created by a collapsed culvert. The presence of the pond has resulted in the thaw of any proximal ice rich Late Pleistocene permafrost and truncated the high resistivity layer. Similarly, a small creek runs through the center of the valley and is prominent in the valley bottom survey where the high resistivity layer is absent (position B in Fig. 4) and instead low resistivity values record a greater presence of liquid water within the sediments (Hilbich et *al*. 2008). Across the entire valley at a depth of 20 to 25 m, a large low resistivity layer is present in each survey marking the depth of the ice-rich permafrost and the presence of either an ice-poor frozen unit or a partially thawed unit.

6 CONCLUSIONS

The detailed borehole and ERT data provide an indication of the distribution of both ice-rich Holocene and Late Pleistocene permafrost within the valley fill. The addition of stable isotopes and radiocarbon dating provide further evidence for the presence of Late Pleistocene permafrost being unconformably overlain by the ice-rich Holocene material. ERT results outline the valley wide distribution of the relict permafrost as highly resistive ice-rich material. Collectively, these results show that complex valley-fill histories and the potential for long term preservation of permafrost even at remarkably warm sites such as the Alaska Highway corridor. Effective highway maintenance along the Alaska Highway relies on the understanding of permafrost distribution surrounding the highway corridor. A combination of borehole data and ERT can provide effective local scale mapping of permafrost along the highway corridor.

ACKNOWLEDGEMENTS

The authors would like to thank the Yukon Research Centre for field support as well as Louis-Philippe Roy and Matt Mahony for assisting with sample collection and analysis. This project was jointly funded by a Natural Science and Engineering Research Council Discovery grant to Duane Froese, Canadian Circumpolar Institute (CCI) grants from Northern Scientific Training Program (NSTP), UofA Northern Awards, Paleoenvironmental Harington Award and a research fellowship form Environorth. Also we are grateful for the in-kind support from Joel Cubley at the Yukon College for lending us the ERT equipment.

REFERENCES

Boaretto, E., Bryant, C., Carmi, I., Cook, G., Gulliksen, S., Harkness, D., Heinemeier, J., McClure, J., McGee, E., Naysmith, P., Possnert, G., Scott, M., van der Plicht, H., and van Strydonck, M. 2002. Summary findings of the fourth international radiocarbon intercomparison (FIRI)(1998–2001) *Journal of Quaternary Science*, 17: 633-637.

Bray, M.T., French, H.M. and Shur, Y. 2006. Further Cryostratigraphic Observations in the CRREL Permafrost Tunnel, Fox, Alaska. *Permafrost and Periglacial Processes*, 17: 233-243.

Burn, C.R., Michel, F.A. and Smith, M.W. 1986. Stratigraphic, isotopic, and mineralogical evidence for an early Holocene thaw unconformity at Mayo, Yukon Territory. *Canadian Journal of Earth Sciences,* 23: 794-803.

Calmels, F., Gagnon, O. and Allard, M. 2005. A Portable Earth-drill System for Permafrost Studies. *Permafrost and Periglacial Processes*, 16: 311-315.

Duk-Rodkin,A. 1999. Glacial limits map of Yukon Territory; Geological Survey of Canada,Open File 3694, Indian and Northern Affairs Canada Geoscience Map 1999-2, scale 1:1 000 000.

Fraser, T.A. and Burn, C.R. 1997. On the nature and origin of “muck” deposits in the Klondike area, Yukon Territory. *Canadian Journal of Earth Sciences,* 34: 1333-1344.

French, H.M. and Shur Y. 2010. The principles of cryostratigraphy. Earth Sciences Reviews, 101: 190-206.

Froese, D.G., 2005. Surficial Geology of Flat Creek (115 O/15) Yukon Territory, Open File 4592. Geological Survey of Canada, Ottawa.

Froese, D.G., Zazula, G.D., Westgate, J.A., Sanborn, P.T., Reyes, A.V., and Pearce, N.J.G. 2009. The Klondike goldfields and Pleistocene environments of Beringia. *GSA Today*, 19: 4-10.

Hilbich, C., Hauck, C., Hoelzle, M., Scherler, M., Schudel, L., Volksch, I., Vonder Muhll, D., and Mausbacher, R. 2008. Monitoring mountain permafrost resistivity tomography: 7-year study of seasonal, annual, and long-term variations at Schilthorn, Swiss Alps. *Journal of Geophysical Research,* 113: 1-12.

Hopkins, D.M. 1982. Aspects of the paleogeography of Beringia during the Late Pleistocene. *In* Paleogeography of Beringia. *Edited by* D.M. Hopkins, J.V. Matthews, Jr., C.E. Schweger, and S.B. Young. Academic Press, New York. Pp. 3-28.

Jackson, L.E., Ward, B., Duk-Rodkin, A. and Hughes, O.E. 1991. The Last Cordilleran Ice Sheet in Southern Yukon Territory. *Géographie physique et Quaternaire,* 45: 341-354.

Jensen, B.J.L., Froese, D.G., Preece, S.J., Westgate, J.A. and Stachel, T. 2008. An Extensive middle to Late Pleistocene tephrochronologic record from east-central Alaska. *Quaternary Science Reviews*, 27: 411-427.

Jensen, B.J.L., Pyne-O'Donnell, S., Plunkett, G., Froese, D.G., Huges, P.M.D., Sigl, M., McConnell, J.R., Amesbury, M.J., Blackwell, P.G., van den Bogaard, C., Buck, C.E., Charman, D.J., Clague, J.J., Hall, V.A., Koch, J., MacKay, H., Mallon, G., McColl, L. and Pilcher, J.R. 2014. Transatlantic distribution of the Alaskan White River Ash. *Geology*, 42: 875-878.

Jensen, M.A., Demidov, I.N., Larsen, E. and Lysa, A. 2009. Quaternary palaeoenvironments and multi-storey valley fills architecture along the Mezen and Severnaya Divina river valleys, Arkhangelsk region, NW Russia. Quaternary Science Reviews, 28: 2489-2506.

Jorgenson, M.T., Romanovsky, V., Harden, J., Shur, Y., O'Donnell, J., Schuur, E.A.G., Kanevskiy, M. and Marchenko, S. 2010. Resilience and vulnerability of permafrost to climate change. *Canadian Journal of Earth Sciences,* 40: 1219-1236.

Kanevskiy, M., Shur, Y., Fortier, D., Jorgenson, M.T. and Stephani, E. 2011. Cryostratigraphy of late Pleistocene syngenetic permafrost (Yedoma) in northern Alaska, Itkillik River exposure. *Quaternary Research*, 75: 584-596.

Kanevskiy, M., Jorgenson, T., Shur, Y., O'Donnell, J.A., Harden, J.W., Zhuang, Q., and Fortier, D. 2014. Cryostratigraphy and Permafrost Evolution in the Lacustrine Lowlands of West-Central Alaska. *Permafrost and Periglacial Processes*, 25: 14-34.

Kennedy, K.E., Froese, D.G., Zazula, G.D. and Lauriol, B. 2010. Last Glacial Maximum age for the northwest Laurentide maximum from the Eagle River spillway and delta complex, northern Yukon. *Quaternary Science Reviews*, 29: 1288-1300.

Kotler, E. and Burn, C.R. 2000. Cryostratigraphy of the Klondike “muck” deposits, west-central Yukon Territory. *Canadian Journal of Earth Sciences,* 37: 849-861.

Lacelle, D., St-Jean, M., Lauriol, B., Clark, I.D., Lewkowicz, A., Froese, D.G., Kuehn, S.C. and Zazula, G. 2009. Burial and preservation of a 30,000 year old perennial snowbank in Red Creek valley, Ogilvie

Mountains, central Yukon, Canada. *Quaternary Science Reviews*, 28: 3401-3413.

Lewkowicz, A.G., Etzelmuller, B and Smith, S. 2011. Characteristics of Discontinuous Permafrost based on Ground Temperature Measurements and Electrical Resistivity Tomography, Southern Yukon, Canada. *Permafrost and Periglacial Processes*, 22: 320-342.

Loke, M.H. and Barker, R.D. 1996. Rapid least-squares inversion of apparent resistivity pseudosections using a quasi-Newton method. *Geophysical Prospecting*, 44: 131-152.

Mackay, J.R., 1973. Reticulate Ice Veins in Permafrost, Northern Canada. *Can. Geotech. Journal,* 11: 230-237.

Murton, J.B. and French, H.M. 1994. Cryostructures in permafrost, Tuktoyaktuk coastlands, western Arctic, *Canada. Canadian Journal of Earth Sciences*, 31: 737-747.

Opel, T., Dereviagin, A.Y., Meyer, H., Schirrmeister, L., and Wetterich, S. 2011. Palaeoclimatic information from stable water isotopes of Holocene ice wedges on the Dmitrii Laptev Strait, northeast Siberia, Russia. *Permafrost and Periglacial Processes*, 22: 84-100.

Reimer, P.J., Bard, E., Bayliss, A., Beck, J.W., Blackwell, P.G., Ramsey, C.B., Buck, C.E., Cheng, H., Edwards, R.L., Friedrich, M., Grootes, P.M., Guilderson, T.P., Haflidason, H., Hajdas, I., Hatte, C., Heaton, T.J., Hoffmann, D.L., Hogg, A.G., Hughen, K.A., Kaiser, K.F., Kromer, B., Manning, S.W., Niu, M., Reimer, R.W., Ricards, D.A., Scott, E.M., Southon, J.R., Staff, R.A., Turney, C.S.M., van der Plicht, J. 2013. IntCal13 and Marine13 Radiocarbon Age Calibration Curves 0-500,000 Years Cal BP. *Radiocarbon*, 55: 1869-1887.

Rampton, V.N. 1978. Surficial geology and geomorphology; Mirror Creek, Yukon Territory. Geological Survey of Canada: Ottawa, ON, Canada.

Reyes, A.V., Froese, D.G. and Jensen, B.J.L. 2010. Permafrost response to last interglacial warming: field evidence from non-glaciated Yukon and Alaska. *Quaternary Science Reviews*, 19: 3256-3274.

Schirrmeister, L., Froese, D.G., Tumskoy, V., Grosse, G., Wetterich, S. (2013). Yedoma: Late Pleistocene ice-rich syngenetic permafrost of Beringia. In: S.A. Elias, The Encyclopedia of Quaternary Science, 3, 542-552.

Smith, M.W. and Riseborough, D.W. 2002. Climate and the Limits of Permafrost: A Zonal Analysis. *Permafrost and Periglacial Processes*, 13: 1-15.

Throop, J., Lewkowicz, A.G. and Smith, S. 2012. Climate and ground temperature relations at sites across the continuous and discontinuous permafrost zones, northern Canada. *Canadian Journal of Earth Sciences*, 49: 865-876.